Soft Robotic Oscillators With Strain-Based Coordination

Steven Ceron, Marta An Kimmel, Alexandra Nilles, and Kirstin Petersen

***Abstract*—Many modular robots and active matter platforms are inspired by natural aggregates of single-celled organisms that exhibit complex emergent behaviors far beyond the capability and range of individuals. These behaviors stem primarily from short range chemical and mechanical interactions. Past work has focused largely on wireless communication akin to chemicals, however, physical interactions require a shift from rigid to soft, durable robots capable of inducing and measuring strain. Here, we present a platform to support such studies. The hardware consists of stand-alone, soft, pneumatic robots capable of radial expansion and contraction. The robots are cheap and fast to produce; they have 3 directional strain sensors, and 6 magnet pairs to loosely couple with their neighbors. We characterize force profiles, sensors, elastic modulus, magnetic interaction, as well as exploratory aggregate motions. Finally, we demonstrate their ability to synchronize, locomote, and fracture in a complimentary quasi-static simulator, with a coupled oscillator model, and discuss evaluation metrics. We hope that this platform will serve to further insights on how simple physical interactions between locally informed agents may lead to complex emergent behaviors.**

***Index Terms*—Swarm robotics, cellular and modular robots, biologically inspired robots.**

I. Introduction

At THE microscale, multicellular organisms often use coupled oscillations to synchronize, disperse, aggregate, and locomote. Popular examples include *Dictyosteliida*, a slime mold where cells coordinate by inducing chemical waves in response to food deprivation [1], and *Trichoplax Adhaerens*, an epitheloid where cells modulate contraction degree and rate to collectively locomote and regulate harmful mechanical stresses [2]. These microorganisms are proof that robustness without global information is possible through a combination of collective physical interactions and local, information-lean signaling. Future robot swarms with limited situational awareness operating in stressful and dynamic environments ranging from the micro- to macro-scale can benefit from studying such emergent behaviors in living collectives, and the mechanisms needed to translate them to simulated and physical robotic hardware.

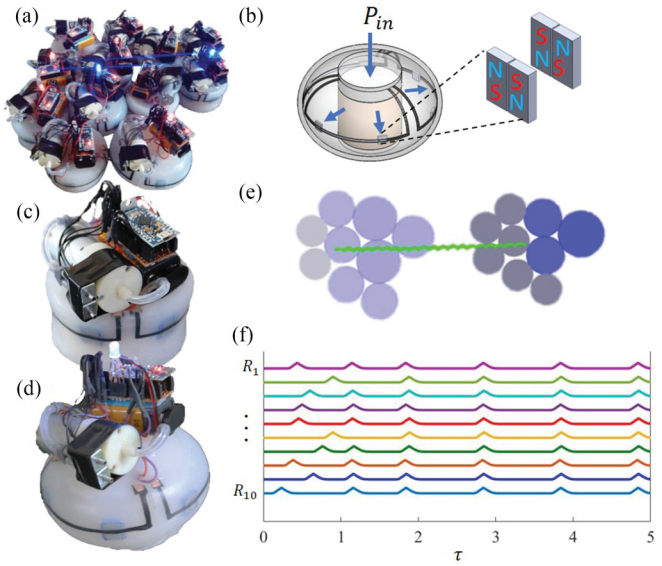

Fig. 1. (a) 12-module Foambot collective. (b) Illustration of an expanded module with 6 magnets and 3 strain sensors able to loosely couple with neighbors, sense its own state and state transitions in neighboring modules. (c)–(d) Module in contracted and expanded state. (e) Simulated modules locomote as a result of traveling waves of expansion and contraction. (f) Module radius over time as 10 out of a 100-module simulated collective synchronize.

To enable such studies, we introduce the Foambots platform consisting of soft, robotic modules capable of coordinating, communicating, and moving by sensing and inducing perturbations and strain in the collective (Fig. 1(a)). The modules couple loosely through 6 magnets embedded in their perimeter. Similar to the *Trichoplax Adhaerens*, the Foambots contract and expand in a 2D plane through fluidic actuation, and use strain sensors on their perimeter to reason about their own state and the actions of their neighbors (Fig. 1(b)–(d)). Beyond accommodating strain-based coordination, the soft modules hold several key advantages over their rigid counterparts. They consist of fewer mechanical parts, and are simple and easy to produce without advanced infrastructure. Compliance facilitates large aggregations with low mechanical tolerance in fabrication. It furthermore ensures safe physical interactions between modules and between modules and external objects. Soft modules may also be used for a wider range of tasks. The soft module

Manuscript received February 24, 2021; accepted July 4, 2021. Date of publication July 29, 2021; date of current version August 13, 2021. This letter was recommended for publication by Associate Editor L. Wen and Editor K.-J. Cho upon evaluation of the reviewers' comments. This work was supported in part by the National Science Foundation under Grants 1933284 and 2042411, in part by a NSF Graduate Research Fellowship, and in part by the Packard Fellowship for Science and Engineering. *(Corresponding author: Steven Ceron.)*

Steven Ceron is with the Sibley School of Mechanical and Aerospace Engineering, Cornell University, Ithaca, NY 14853 USA (e-mail: stevenceron100@gmail.com).

Marta An Kimmel, Alexandra Nilles, and Kirstin Petersen are with the School of Electrical and Computer Engineering, Cornell University, Ithaca, NY 14853 USA (e-mail: mak454@cornell.edu; aqn3@cornell.edu; kirstin@cornell.edu).

Digital Object Identifier 10.1109/LRA.2021.3100599

membrane can deform to fill gaps, and the collective can change its overall stiffness both as a function of module density and as a function of module expansion state. We have prioritized these design features as a first step toward applications such as active bio-medical stents or mobile retaining structures, such as temporary dams.

The remainder of this article discusses related work and details hardware design, fabrication, characterization, and exploratory experiments, alongside a coupled oscillator algorithm to produce emergent behaviors in a custom simulator (Fig. 1(e)–(f)). We hope this platform will further research on and serve as a low-barrier of entry to the study of physical interactions in the collective robotics realm.

II. Related Work

The Foambots platform is related to two, largely separate bodies of work in literature. The first is *active matter*, where simple oscillating robots leverage statistical mechanics to produce global behaviors from local physical interactions, such as motion or synchrony [3]–[5]. Most notably, the Particle robots used rigid components and statistical mechanics demonstrating directed motion by phase locking their oscillations to a global signal [3]. In contrast to these robots, the Foambots are designed for studies of local coordination via strain, and additionally benefit from soft material properties as described earlier.

The second body of work is *modular robots*, where physically connected agents reason deliberately about how to produce collective behavior. Modular robots inspired by natural cells was first proposed by Fukuda [6], and has since the introduction of soft robots been followed up by a wealth of examples of soft modular cubes in rectilinear lattice formations, [7], [8] just to name a few. These studies often focus on producing peristaltic locomotion or conveyor belt transport of other objects. As is true for most soft robots, the majority still rely on external power or pressure, and none have coupled sensing and actuation. They typically rely on either manual assembly leading to fixed topologies, or loose magnetic coupling which can be cumbersome as connecting tubes and wires tangle. As alternatives to pneumatics, [9] leveraged passive deformations in flexible PCBs, and switchable magnets to produce collective motion. [10] demonstrated magnetically coupled tensegrity modules capable of collective motion with a specific focus on ease of assembly and pre-emptive stiffness tuning. Finally, although some robot collectives have shown coordination through physically transmitted vibrations [11], [12], none have the coupled strain actuation and sensing which is key to coordination in e.g. *Trichoplax Adhearens*.

III. Foambot Fabrication

A Foambot module consists of a rigid electronic core resting on top of a poro-elastic foam which is surrounded by a polymer pocket that can expand radially upon pressurization. The hardware was designed with accessibility in mind: fabrication requires little know-how or specialized equipment beyond a soldering station and a well-ventilated space. Each Foambot module can be fabricated with ∼3 hours of active time and

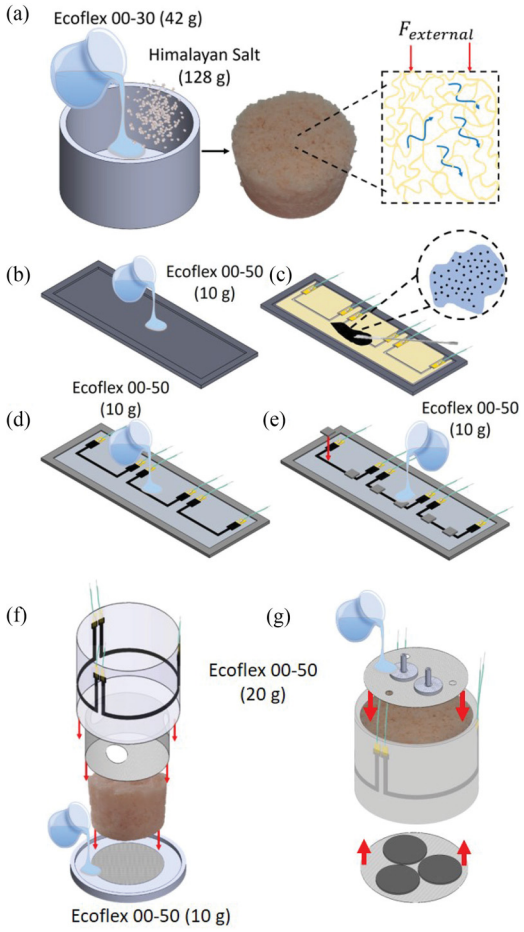

Fig. 2. Module fabrication. (a) Poro-elastic foam with 65% porosity. (b)–(e) Carbon composite sensor with embedded magnets on the outer membrane. (f) Poro-elastic foam wrapped in an inner strain-limiting layer and an outer membrane. (g) Top strain-limiting layer and bottom 3D-printed sliders.

∼5 hours of curing time. In our case, we molded four modules simultaneously with only a marginal increase in production time.

The poro-elastic foam core gives the soft robot structural integrity, while allowing fluid to flow throughout its volume to the outer cavity. The core is created through a salt-loss process (Fig. 2(a)), where Himalayan salt (grain diameter = 1 - 3 mm) is mixed with Ecoflex^{TM} 00-50 before setting and is then dissolved after the silicone has set. The salt grains are well-packed such that the resulting pores are interconnected, thus allowing fluid to flow through its volume. Once cured, the core is wrapped by a strain-limiting layer that creates a barrier between the internal porous pocket and the outer cavity. The strain-limiting layer is fabricated by pouring Ecoflex 00-50^{TM} into a mold with a piece of laser-cut fabric. The holes along the length of the strain-limiting layer allow air to flow to the external cavity.

The stretchable outer membrane encompasses 6 magnet pairs and 3 resistive strain sensors (Fig. 1(b)). The magnets enable modules to aggregate loosely. The sensors enable sensing of three event types: modules can sense the extent of their own expansion; they can sense when new neighbor attachments form; and they can detect when attached neighbors start to expand. By

including three separate strain sensors, modules have a coarse sense of directionality.

The outer membrane is fabricated by first pouring a 1 mm thick layer of Ecoflex™ 00-50 into a rectangular mold. After the first layer has set, a stencil paper is placed on top of it. Copper-taped electrodes are soldered to silicone wires and adhered to the Ecoflex™ 00-50 surface using Silpoxy™. A hand-mixed Carbon composite is spread across the surface of the stencil. The Carbon composite is composed of Carbon Black powder and Ecoflex™ 00-30, part A, with a mass ratio of 1:6 [13]. A second 1 mm thick layer of Ecoflex™ 00-50 is added on top. When the second layer has set, we adhere the six magnet pairs with equal spacing using Silpoxy™, and firmly embed the magnets in the membrane through another thin layer of Ecoflex™ 00-50. The pairs consist of two magnets oriented in opposite directions to ensure that modules can attach in any orientation. Each magnet is made of NdFeB (Grade N52) material with a surface field of 3114 Gauss. Upon completion, the membrane is wrapped around on itself to form a cylinder. The membrane is positioned such that the gap between its two ends can be filled by Ecoflex™ 00-50 (Fig. 2(b)–(e)).

Finally, the outer membrane is positioned around the poro-elastic foam (Fig. 2(f)–(g)). The inner strain-limiting layer and the outer membrane are placed flush with the bottom of the foam, wrapped around it, and the ends are glued with Silpoxy™. Ecoflex™ 00-50 is poured into a mold to form a 2 mm thick layer at the bottom of the module. The upper edge of the outer membrane is then folded inward and glued against the inside of the strain-limiting layer with SilPoxy™. A circular strain-limiting layer (embedded in Ecoflex™ 00-50) is placed on top of the foam and glued to the folded membrane sides. After the SilPoxy™ sets, Ecoflex™ 00-50 is poured on the top to create a 15 mm layer that restricts upward expansion. The bottom strain-limiting layer and sliders (printed in Veroblue with a Stratasys Objet 3D printer with 300 μm resolution) are glued to the bottom of the module. The sliders reduce friction, enabling easy testing of the collective on a variety of surfaces.

To control the Foambots, the core electronics consist of an Arduino Pro Micro, an Uxcell 6 V miniature air pump, two Uxcell 5 V mini solenoid valves coupled in parallel, an RGB LED for debugging, and a 9 V battery (Fig. 3(a)).

IV. Foambot Characterization

A. Actuation

The Foambot modules actuate through expansion and contraction of their outer membrane. During inflation, the outer membrane exhibits an approximately linear increase in radius; this behavior is mirrored during depressurization (Fig. 3(b)). The full actuation cycle consists of an expansion period, a contraction period, and a rest period. Given the particular pump and membrane elastic modulus, we found the following parameters to provide significant changes in properties, while limiting adverse material effects: By running the pump for $T_{exp} = 7$ s, we see 21% increase in radius from $R = 42$ mm to 51 mm, a notable amount of strain amongst soft sensors and actuators. From a fully inflated state, in isolation, it takes $T_{con} = 12$ s for the module to deflate to ambient pressure. Further, to enhance sensor signal to noise ratio as discussed in the following section, we normally add a rest period after an expansion and contraction cycle where the module remains passive ($T_{rest} = 19$ s). Note that the radial expansion creates pressure distribution on the surroundings, which allows the module to perform work on itself or on others, depending on the balance between its own pushing force and the static friction force of its neighbors.

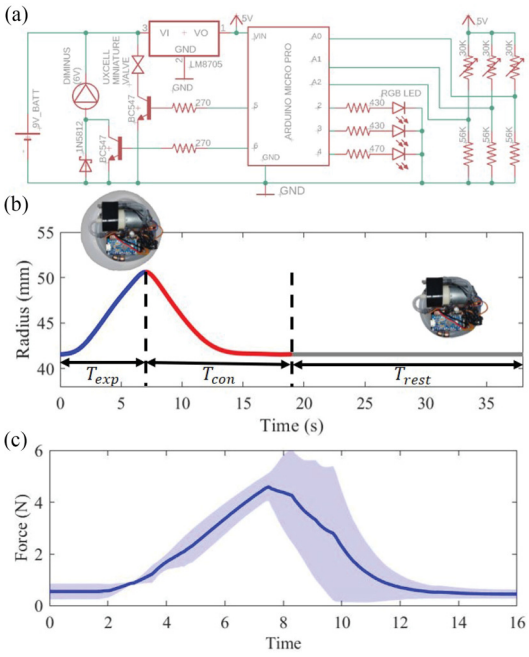

Fig. 3. (a) Module driver schematic. (b) The oscillatory cycle of a module with $T_{exp} = 7$ s, $T_{con} = 12$ s, and $T_{rest} = 19$ s. The inserts show the module top view at full expansion/contraction. (c) Pushing force exerted on a strain gauge by a module with $T_{exp} = 6$ s and $T_{con} = 10$ s.

B. Acting Forces

Three forces dominate movement in a Foambot collective - magnetic attraction, pushing forces, and frictional forces with the floor. A module will slide across a surface making or breaking connections with neighboring modules if the combined magnetic and pushing forces acting on it are greater than its frictional force. Note that the relative magnitude of each of these forces is an interesting line of study that we leave for future investigations.

We measured the magnetic holding force between two magnet pairs embedded in Ecoflex™ 00-50 to be 2.38 ± 0.33 N (n = 10). This was measured by fixating one to a load cell (Adafruit, 5 kg), while pulling the other away with a linear actuator. Fig. 3 (c) shows the pushing force during module expansion. Note that the contraction cycle shows more variation due to slight differences in the valves and membrane thicknesses. When measured for a module with $T_{exp} = 6$ s, with a maximum radial expansion of 13% the force reached 4.6 ± 0.54 N. We performed this experiment by placing the module at rest between two walls, one fixed, another connected to the aforementioned load cell.

Due to their slow movement, module friction with the floor is largely static. The static coefficient of friction between a

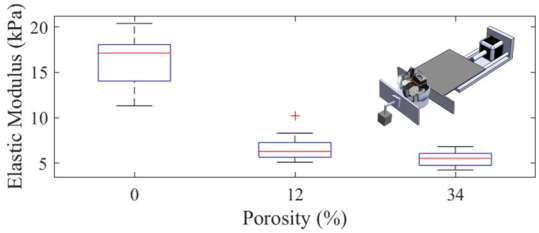

Fig. 4. Compression tests of a single module (n = 15).

module's sliders and different surfaces was found by connecting a module to one end of a string on a pulley and adding load to the other end until the module began to move. These experiments were done with five different modules (each weighing approximately 250 g) for a wooden table surface, a Styrofoam surface, and a white board plane; the resulting static coefficients of friction were determined to be 0.27 ± 0.01, 0.52 ± 0.11, and 0.29 ± 0.03, respectively. Each of these surfaces is common to research labs where algorithms for planar, modular robots can easily be tested across different terrains.

C. Deformation

As previously discussed, the softness of the modules paves the way for a range of interesting studies. Interestingly, as the modules inflate, their elastic modulus decreases. When at ambient pressure, modules have an elastic modulus given by the internal poro-elastic foam wrapped by membranes of Ecoflex^{TM} 00-50. As the module expands, it effectively creates more open space in the outer cavity decreasing the effective elastic modulus, similar to the way poro-elastic foams with increasing porosities reduce their effective elastic modulus. To characterize this property we performed compression tests on a single module located between one plate connected to a linear actuator and another mounted with a load cell (Adafruit, 5 kg) to determine the applied force. We assumed a constant area for determining stress, equal to the cross-sectional area given at the module's center. Although the area of interest changes with applied stress, we found that this approximation matched the general profile found in poro-elastic foams compressed using an Instron machine.

D. Sensing

The three sensors on the Foambots facilitate strain-based coordination. These sensors exhibit greater electrical resistance as their length increases and when they are squeezed. The former is most pronounced when modules expand; the latter depends on the acting forces between neighboring modules, e.g. during expansion, and any magnetic connections. To measure their value, each strain sensor is connected in a half-bridge Wheatstone configuration. We characterized the sensor performance in terms of repeatability, consistency over time, and the mechanical coupling between them on both passive and active modules.

Fig. 5(a) shows the raw resistance versus module radius over 10 expansion/contraction cycles for two sensors. While the absolute value and range of resistance varies due to the inexpensive, manual fabrication process, the general profile is qualitatively similar.

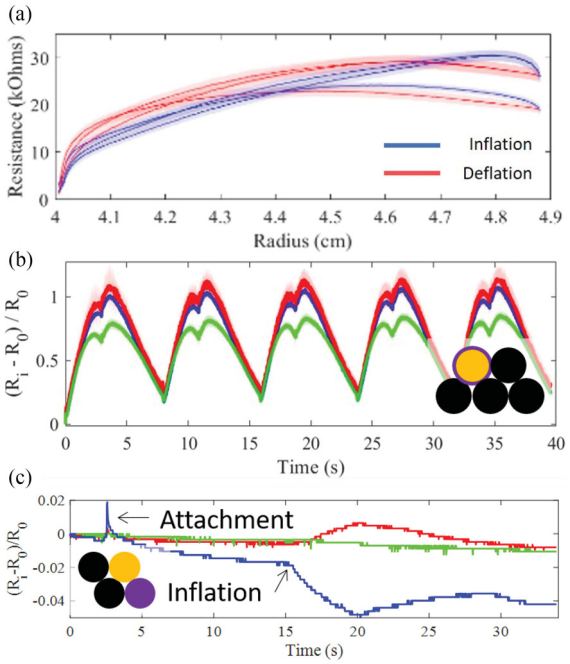

Fig. 5. (a) Output from two sensors embedded on a module oscillating 10 times. (b) Normalized sensor outputs from an oscillating module (yellow) with four neighbors (black). In (a) and (b), solid lines and shaded regions represent mean and standard deviation respectively. (c) Normalized sensor outputs from a passive module (yellow) with two passive neighbors (black), and one module (purple) attaching and oscillating.

Fig. 5(b) shows the normalized sensor output for all three sensors on an active module with four passive neighbors arranged as shown in the insert. This data demonstrates the repeatability of the resistance-strain relationship over time. Again, we note that the range varies between sensors, but the qualitative behavior is similar and stays constant over multiple oscillation cycles. Specifically, the signal dips toward the end of the expansion period, a feature that is apparent at approximately the same strain ($\sim$1.2 mm / mm) across all sensors, and is mirrored at the beginning of the deflation period ($\sim$1.3 mm / mm). This could be attributed to the gel-like nature of the Carbon composite: a lower strain value might break up some of the electrical pathways and increase resistance; a strain higher than a given threshold might cause the gel to move around slightly within the Ecoflex^{TM} membrane and repair electrical pathways and decrease resistance. Further tests exploring these sensors would be needed to confirm this.

We tested the ability of a module to detect new module attachments and neighboring expansions (Fig. 5(c)). Because of sensor variability, and because their signal changes depending on whether one or two modules are connected over their length, we distinguish between the two events as follows. Attachments were detected by checking if the change in raw sensor output over 100 ms was greater than 4 bits. Inflations were detected by doing a complementary low pass filter on the change in raw sensor output (alpha = 0.5), and checking for a change

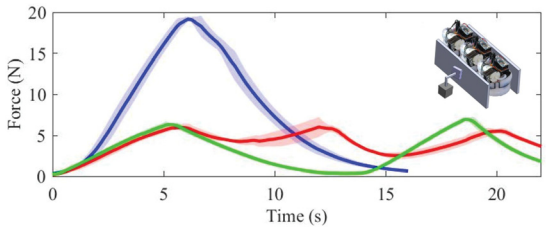

Fig. 6. Force exertion by three modules ($T_{exp} = 6$ s, $T_{con} = 10$ s, $T_{rest} = 0$ s), when they are synchronized (blue), and out of phase by $\sim 70°$ (red) and $135°$ (green), respectively.

greater than 3.2 bits over 1 s. To eliminate multiple detections triggering in a row, we omit detections occurring up to 5 s after an inflation has been triggered. Normally, at this time, the sensing module would itself be inflating and consequently ignore new events anyway. We tested this method with three sensors over 30 attachments and 30 expansion cycles, in a three and six consecutive neighbor configuration. All attachments were detected with a 0.14 s ± 0.08 s delay. 27 out of 30 inflations were detected with a 1.08 s ± 0.56 s, as well as 5 false positives and 1 false negative. Four of the false positives occurred on sensors that were not connected to the expanding module.

We further found that the sensors have a low signal to noise ratio while the onboard pump is running. This is due to both direct noise coupling in the shared power supply, and because the loop configuration of the strain sensors pick up electromagnetic interference. Therefore, modules can effectively only sense strain when the module is not expanding. Although this is limiting, this concept has precedence in natural collectives, where, e.g. large networks of neurons can create emergent behavior in spite of refractory periods occurring after individual action potentials.

V. Foambot Collectives

The advantage of a single Foambot stems from coupled sensing and actuation and its ability to elastically deform. An aggregate of modules can collectively leverage these simple functionalities to produce emergent collective behaviors such as collective force exertion, locomotion, and fracture (Fig. 7). Using up to 9 modules, we demonstrate that each of these behaviors are feasible with the current hardware and encourage the reader to look at the accompanying video. Note that we leave it to future work to incorporate full feedback behavior on the hardware, and that these videos represent hard-coded cycles. In the next section, we expand on how decentralized algorithms for these robots might work through a quasi-static simulation framework.

Fig. 6 demonstrates how synchronized modules may push in unison to achieve greater force exertion. Using the same 5 kg load cell setup mentioned in Section IV-B, we found that three modules connected in parallel could exert more than three times the force feasible when out of phase.

Collective motion appears when the following conditions on the module pushing force are satisfied: it must be greater than its static friction force and less than the summed static friction force of the modules that actuate after this module. Figs. 7(a)–(b) show the ability of Foambots to locomote collectively through waves of expansion and contraction traveling opposite the module motion. We found that 3 modules move $\sim$0.1 robot radii per cycle, and 9 modules move $\sim$0.125 robot radii per cycle. Note that in the latter experiment, the top left module is left behind. This is caused by the combined pushing force of several modules along the diagonal expanding together; the module is pushed out such that it breaks a connection with one of the modules and can then not join back with the collective as the group moves away, severing its second connection. This example highlights 1) that the aggregate is robust to loss of individuals and 2) the need to carefully couple neighboring oscillations to avoid unwanted fractures.

As previously indicated, the choice of Foambot magnets will affect the collective behavior. Strong magnets allow experiments without fracture; however, weak magnets facilitate loose magnetic coupling and reconfiguration which may be used advantageously to overcome environmental geometric constraints or to converge on more stable collective morphologies (tight circle packing). Emergent behaviors based on these low-level physical interactions are predominantly dependent on the number of modules, the starting configuration of the collective, the balance between attractive and frictional forces, and the amplitude and synchrony of radial expansion. As shown throughout the videos summarized in Fig. 7, the slow movement of these modules enables most broken connections to be repaired. In cases where different sections of the collective are moving in opposing directions, the appearance of larger fractures may be reduced with greater connection density and appropriate actuation patterns.

VI. Simulation and Metrics

To support algorithmic development, we wrote a custom simulation framework based on Matlab and / or the free alternative Octave Online. The simulation includes the ability of modules to expand and contract radially and detect when neighboring modules transition between states. It also includes collision checking, pushing forces, static friction, and magnetic forces. Informed by experiments and COMSOL simulations, the latter was incorporated as a decaying function with a maximum force capped at 2.4 N at separation distances ≤ 0.38 module radii, and a minimum of 0 N at a distance greater than 1 module radii. Incorporation of module deformations is left for future work.

Inspired by the rich literature on coupled oscillators dating back to the basic Winfree model [14], we suggest three metrics to evaluate the emergent behavior of the collectives:

Global coherence: the average coherence of phases amongst all modules. This is a dimensionless value between 0 and 1:

$$Z_G = \frac{1}{N}\left|\sum_{j=1}^{N} e^{i\theta_j}\right| \tag{1}$$

Local coherence: the average coherence of phases amongst neighboring modules. This is a dimensional value between 0 and 1, where m is the iterative counter for the total number of modules and n is the number of neighbors around a given

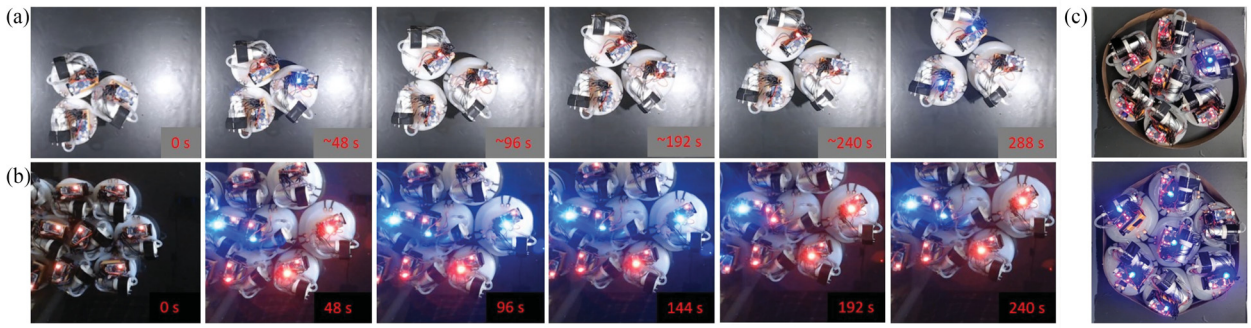

Fig. 7. (a)–(b) Snapshots from movie showing locomotion in the uper right direction of 3 and 9 modules when there are traveling waves in the opposite direction. (c) 7 synchronized modules expand and fill the space in a constraining membrane. Blue light signifies expansion, red contraction, and blank rest.

module:

$$Z_L = \frac{1}{N}\sum_{m=1}^{N}\left[\frac{1}{n}\left|\sum_{\langle j\rangle}^{n} e^{i\theta_j}\right|\right] \tag{2}$$

Linear momentum: the collective motion:

$$P = \frac{1}{N}\left|\sum_{i=1}^{N}\dot{x_i}\right| \tag{3}$$

Throughout these metrics, N is the total number of modules in the collective, θ_j is the phase of a given module, and $\dot{x_i}$ is the change in module position.

A high global coherence means all modules share the same phase; however, it is much more common to encounter scenarios where there is low global coherence and high local coherence due to fractures appearing in the collective. Along the same track, a high linear momentum means that the collective moves in the same direction, which implies that the collective most likely remains connected. A low linear momentum could also mean that the collective has broken into multiple clusters, each possibly moving in a different direction.

VII. Coupled Oscillator Algorithm

To demonstrate how modules may achieve emergent behavior, we took inspiration from past work on static coupled oscillators [14], [15]. Specifically, we modified the original model, such that modules maintain equal natural frequency, and a constant T_{exp} and T_{con}, adjusting only their T_{rest} to achieve collective oscillatory patterns. More specifically, modules map their actuation cycle to a phase value as shown in line 2 of Algorithm 1. Here, τ_i is the time since the cycle of module i began, A_i is the actuation state (-1 for contraction, 1 for expansion, and 0 for rest).

Algorithm 1 describes how modules adjust their cycles, and the behavior is further illustrated in Fig. 8, through radial profiles of two interacting modules. The algorithm uses a coupling factor, $K \in (0, 1)$, as a "knob" to control the behavior of the collective. When a neighboring activation is detected, an agent at rest will update its phase value by an amount proportional to the phase difference between itself and the activating neighbor, scaled by K. See line three of Algorithm 1 for the exact expression.

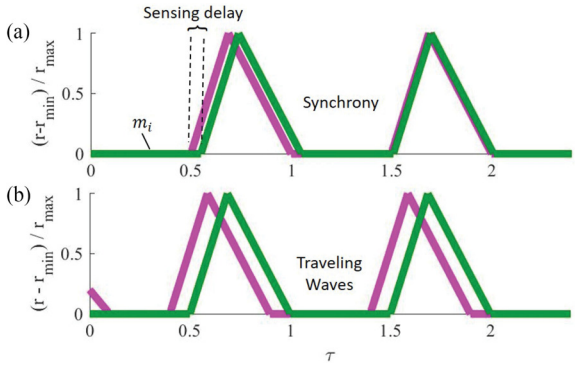

Fig. 8. Graphical representation of modules' behavior when a sensing module (green) responds to a neighboring module's (purple) expansion. (a) The coupling factor K is sufficiently high that it brings two modules to synchrony within one cycle. (b) The sensing module maintains a phase offset with its neighbor, enabling traveling waves of actuation.

When a neighbor inflates, the "listening" module calculates a new phase value $\theta_i(\tau_i)$ as a function of the coupling factor and its phase difference with module j. Our algorithm allows for two possible cases: if the new phase is over the expansion threshold, the module at rest immediately begins to expand and sets $\theta_i(\tau_i) = 0$. In the second case, the phase update does not yet require expansion, but the resting module still shortens the amount of time it stays at rest. Intuitively, increasing K increases synchrony by causing the jump in phase to increase, bringing modules closer in phase to their neighbors during an inflation event.

To demonstrate the range of behaviors that can emerge from this algorithm, we evaluated our metrics over a range of values of K and the number of modules in a rectangular 10-module tall configuration. Fig. 9(a)–(b) demonstrate synchronization as the global and local order parameters increase with increasing K. A snapshot of 10 modules within a 100 module collective synchronizing is also shown in Fig. 1(f). Fig. 9(c) demonstrates locomotion, caused by asynchronous patterns of activation leading to higher linear momementum for lower values of K and smaller collectives. Fig. 9(a) and b show higher local than global coherence, indicating fracture. At high numbers of modules, the collective may form fracture lines that split the modules into

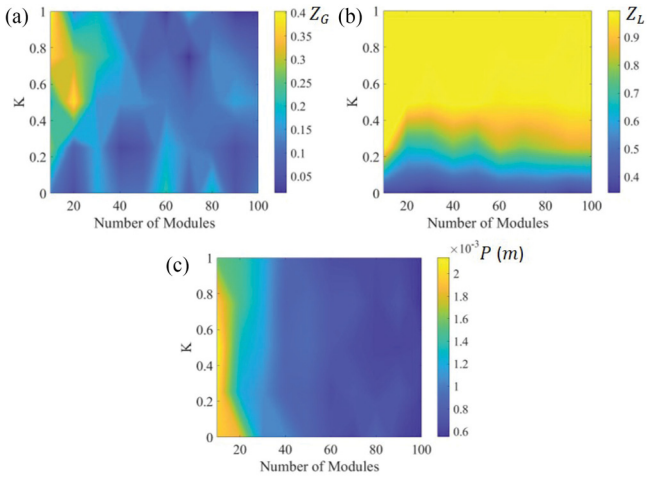

Fig. 9. Algorithm 1 applied to 10 - 100 module collectives in a rectangular configuration. Results are averaged over 20 simulations. (a) Global Coherence (Z_G). (b) Local coherence (Z_L). (c) Linear momentum (P).

Algorithm 1: Coupled Oscillator Algorithm.

if $A_j = 1$ and $r_j \sim r_{min}$ **then**
  $\theta_i(\tau_i) = \frac{\tau_i}{T_{exp}+T_{con}+T_{rest}}$
  $\theta_i(\tau_i + dt) = \theta_i(\tau_i) + K(\theta_i(\tau_i) - \theta_j(\tau_i))dt$
end if
if $t_i^s \neq 0$ **then**
  if $A_i = 0$ and $\theta_i(\tau_i)T/(2\pi) < T_{exp} + T_{con}$ **then**
    $A_i = 1, \tau_i = 0$
  else if $A_i = 1$ and $\tau_i = T_{exp}$ **then**
    $A_i = -1$
else if $A_i = -1$ and $\tau_i = T_{exp} + T_{con}$ **then**
    $A_i = 0$
  end if
end if

multiple groups and thus lead to high local coherence but low global coherence.

VIII. Summary

We introduced a soft robot to enable studies on strain-based coordination of robot collectives, following inspiration from natural systems. This system is unique in that modules directly couple actuation and signaling to coordinate locally. We demonstrated the effects of synchrony, locomotion, and fracture in 9 real modules and up to 100 simulated modules as coupled oscillators. In the future, we intend to leverage this platform to demonstrate robust emergent behaviors through local interactions on the real robots. Given the extreme simplicity of these robots and the strain-based coordination mechanism, insights from these studies may pave the way for robust emergent behavior in robot swarms interacting physically at the micro- to macro-scale.

Acknowledgment

The authors would like to thank Danna Ma, Haron Abdel-Raziq, and Jacob Peters from Cornell University, for fruitful discussions on the hardware design and bio-inspiration.

References

[1] J. Kim, P. Heslop-Harrison, I. Postlethwaite, and D. G. Bates, "Stochastic noise and synchronisation during dictyostelium aggregation make camp oscillations robust," *PLoS Comput Biol*, vol. 3, no. 11, p. e 218, 2007.
[2] S. Armon, M. Storm, A. Aranda-diaz, and M. Prakash, "Ultrafast Epithelial Contractions Provide Insights Into Contraction Speed Limits and Tissue Integrity," *Proc. National Acad. Sci.*, vol. 115, no. 44, pp. E10333-E10341, 2018.
[3] S. Li *et al.*, "Particle robotics based on statistical mechanics of loosely coupled components," *Nature*, vol. 567, no. 7748, pp. 361–365, 2019.
[4] W. Zhou and N. Gravish, "Density dependent synchronization in contact-coupled oscillators," 2020, *arXiv:2012.07124* .
[5] S. Shrivastava *et al.*, "Material remodeling and unconventional gaits facilitate locomotion of a robophysical rover over granular terrain," *Sci. Robot.*, vol. 5, no. 42, 2020.
[6] T. Fukuda, "Self organizing robots based on cell structures-cebot," in *Proc. IEEE Int. Workshop Intell. Robots Syst.*, 1988, pp. 145–150.
[7] S. Yim and M. Sitti, "Softcubes: Towards a soft modular matter," in *Proc. IEEE Int. Conf. Robot. Automat.*, 2013, pp. 530–536.
[8] X. Sui, H. Cai, D. Bie, Y. Zhang, J. Zhao, and Y. Zhu, "Automatic generation of locomotion patterns for soft modular reconfigurable robots," *Appl. Sci.*, vol. 10, no. 1, p. 294, 2020.
[9] N. J. Wilson, S. Ceron, L. Horowitz, and K. Petersen, "Scalable and robust fabrication, operation, and control of compliant modular robots," *Front. Robot. AI*, vol. 7, p. 44, 2020.
[10] D. Zappetti, S. Mintchev, J. Shintake, and D. Floreano, "Bio-inspired tensegrity soft modular robots," in *Proc. Conf. Biomimetic Biohybrid Syst.*. Springer, 2017, pp. 497–508.
[11] R. M. McKenzie, M. E. Sayed, M. P. Nemitz, B. W. Flynn, and A. A. Stokes, "Linbots: Soft modular robots utilizing voice coils," *Soft Robot.*, vol. 6, no. 2, pp. 195–205, 2019.
[12] M. Malley, B. Haghighat, L. Houe, and R. Nagpal, "Eciton robotica: Design and algorithms for an adaptive self-assembling soft robot collective," in *Proc. IEEE Int. Conf. Robot. Automat.*, 2020, pp. 4565–4571.
[13] D. Ma, S. Ceron, G. Kaiser, and K. Petersen, "Simple low-cost fabrication of soft sensors for feature reconstruction," *IEEE Robot. Automat. Lett.*, vol. 5, no. 3, pp. 4049 –4054, Jul. 2020.
[14] A. T. Winfree, "Biological rhythms and the behavior of populations of coupled oscillators," *J. Theor. Biol*.
[15] M. R. E. and S. S. H., "Synchronization of pulse-coupled biological oscillators," *SIAM J. Appl. Math.*, vol. 50, no. 6, 1990.